Consolidation of Molybdenum nanopowders by spark plasma sintering: Densification mechanism and first mirror application

Geuntak Lee, Charles Manière, Joanna Mckittrick, Russell Doerner, Daisuke Nishijima, Anthony Gattuso, Tyler Abrams, Dan Thomas, Christina Back, Eugene A. Olevsky

Consolidation of Molybdenum nanopowders by spark plasma sintering: Densification mechanism and first mirror application

Geuntak Lee

Charles Manière

Joanna McKittrick

Russell Doerner

Daisuke Nishijima

Anthony Gattuso

Tyler Abrams

Dan Thomas

Christina Back

Eugene A.Olevsky

Abstract

Mo nanopowders are synthesized by ball milling and the following hydrogen reduction of MoO3 powders. The densification mechanism of Mo nanopowders during spark plasma sintering (SPS) is analyzed by the combination of the regression of the experimental data on regular SPS and on the SPS multistep pressure dilatometry based on the continuum theory of the sintering. The Mo mirror with 400 nm average grain size and 93% relative density is fabricated by the SPS. The performance of the mirrors made from a single crystal Mo and from the hydrogen-reduced sintered Mo nanopowder is discussed. The microstructure and optical properties of the mirrors are characterized before and after plasma exposure, and no substantial degradation of the reflectivity was observed.

Keywords

MolybdenumDensification mechanismDiagnostic mirrorsITERReflectivity

1. Introduction

Metallic mirrors are planned as part of diagnostic systems which relay optical signals from the plasma to measurement devices for the International Thermonuclear Experimental Reactor (ITER) [1]. First mirrors (FM), those in close proximity or direct sight line of the ITER plasma, will be subject to harsh environmental conditions that deteriorate their reflectivity and performance. Molybdenum (Mo) has been utilized as a FM material due to its low sputtering yield under plasma sputtering conditions [2]. Single crystal (SC) Mo mirrors have shown the best performance under erosion intensive conditions characteristic for fusion plasmas. However, the technology to fabricate large-format SC mirrors

(>∼120 mm diameter), needed for ITER, is not commercially available. Eren et al. [3] fabricated nanocrystalline (NC) metallic mirrors with 70 nm–100 nm grain size by Mo coating (thickness of 1 μm) onto a polished stainless steel substrate using magnetron sputtering. The spectral reflectivity performance of the NC mirror was comparable with a SC Mo mirror [4]. Sintered NC Mo is a candidate process for large-format FMs due to lower cost than that of SC, comparable performance, and improvement in mechanical performance over coated substrates. Also, a bulk Mo metal mirror made by sintering should have the longer life expectancy than the one made by the coating method, which requires long time and high price to produce a thick metal mirror. Therefore, the sintering of a Mo metal mirror with nanoscale grain size should be explored.

The fabrication method of Mo metal mirror with a grain size less than 1 μm and with greater than 90% relative density is difficult due to the large grain growth of metal nanopowders during sintering. Srivatsan et al., showed that the densification of Mo nanopowders (100 nm) using plasma pressure compaction method resulted in grain size of 1 μm–3 μm with 97% relative density. Apparently, only Park et al. [5], obtained the Mo compact with ultra-fine 500 nm grain size with 90% relative density using a two-step sintering method with 20 h holding time. Also, the description of the fabrication of the Mo mirrors by the sintering route tested for reflectivity is limited in the literature [4,6,7]. Voitsenya et al. [8] indicated the possibility to make Tungsten (W) and Mo mirrors with 250 nm–350 nm grain size using resistance sintering and provided the reflectivity results, however, only W sintering conditions were described [9]. To advance the research on the fabrication of metal mirrors for nuclear engineering applications and to fabricate bulk metal mirrors with nano-size grains (<100 nm), the study of the densification behavior for Mo nanopowders is required.

The commercial Mo nanopowders made by the wire explosion method [10] suffer from two disadvantages: large surface oxidation during handling and storage and broad particle size distribution from 50 nm to 2 μm. These powder properties prevent the fabrication of Mo pellets with nano-size grains. Kim et al. [11,12], showed the densification behavior of Mo nanopowders fabricated from the milled MoO_3 by H_2 reduction. Freshly synthesized Mo nanopowders using this method showed narrow particle size distribution with an average particle size of 100 nm.

In the present study, for the first time, the NC Mo disks with an average grain size of 400 nm were fabricated by SPS. Sintering kinetics was analyzed using the in situ methods [13] of the determination of the sintering constitutive parameters based on regression analysis of the porosity evolution curves by the continuum theory of sintering [[14], [15], [16]]. The reflectivity and microstructure of the SC and NC Mo mirrors were evaluated before and after plasma exposure using the PISCES-A linear plasma device.

2. Sintering mechanism determination

Each of the densification mechanisms corresponding to the powder material high-temperature deformational behavior relates to specific values of the creep exponent (n) and creep activation energy (Q), by which the mechanism can be defined uniquely [[17], [18], [19]]. This chapter of the paper focuses essentially on the determination of Q and n which represent not a single sintering mechanism but an indication of which mechanism is dominant. The value of n is an indicator of the degree of non-linearity of the sintering behavior.

The direct in situ method based on the continuum theory of sintering [15] is used here to identify the densification mechanism for Mo nanopowders. The continuum model we use assumes the porous material's creep behavior. Compared to theoretical models which take into account the neck size and the porous body skeleton's volume, our model includes these contributions in equivalent creep parameters and in the mechanical shear and bulk moduli. The grain growth impacts the sintering mechanism and can be included in the consistency term. To minimize the grain growth effect, we explore the relative density range where the grain growth does not occur (<87% of the relative density).

Initially, the regression analysis gives the temperature dependent creep parameter values (A0 (pre-exponential constant of power-law creep equation (K/(s Pan)), Q (kJ/mol) and n) based on the SPS test conducted at the ramping temperature and assuming traditionally used expressions for the compaction moduli [14]. When n value cannot be unambiguously determined by the regression analysis, the SPS multistep pressure dilatometry approach is used [16]. The detailed derivation of the sintering parameters can be found elsewhere [13,14].

For the purpose of the regression analysis, the linearization of the constitutive equation of the pressure-assisted sintering [15] can be expressed as follows:

$$n \ln \left(\frac{|\sigma_z|}{\left(\psi + \frac{2}{3}\varphi\right)^{\frac{n+1}{2n}} (1-\theta)^{\frac{n-1}{2n}} |\dot{\varepsilon}_z|^{\frac{1}{n}}} \right) - \ln(T) = \ln(A_0) + \frac{Q}{RT} \tag{1}$$

where φ is the normalized shear modulus, ψ is the normalized bulk modulus, is the applied axial stress (Pa), is the strain rate of the sample (s−1), θ is the porosity, T is the temperature (K), and R is the gas constant (J/mol K).

For each n value, various theoretical porosity evolution curves can be plotted using the obtained creep parameters (A0, Q) based on the constitutive equation of sintering assuming the same experimental sintering conditions (T and) [15], and these curves can be compared with the experimental porosity evolution data. However, in many cases the determination of the parameter n value is challenging due to its limited sensitivity affecting the accuracy of this parameter's determination [13]; therefore sometimes the supplementary step (SPS multistep pressure dilatometry approach, in this study) is necessary to determine the n value.

Using the SPS multistep pressure dilatometry [16], the n value can be determined by the following equation:

$$n = \frac{\ln \left(\frac{\exp(-|\varepsilon_{z2}|) - (1-\theta_0)}{\exp(|\varepsilon_{z1}|)} \frac{|\dot{\varepsilon}_{z1}|}{(1-\theta_0)} \frac{|\dot{\varepsilon}_{z1}|}{|\dot{\varepsilon}_{z2}|} \right)}{\ln \left(\frac{\sigma_{z1}}{\sigma_{z2}} \exp(|\varepsilon_{z2}| - |\varepsilon_{z1}|) \sqrt{\frac{\exp(|\varepsilon_{z2}|) (1-\theta_0)}{\exp(|\varepsilon_{z1}|) (1-\theta_0)}} \right)} \tag{2}$$

where the indices 1 and 2 indicate the different compressive strain and strain rates and stress before and after the pressure jump, and is each initial porosity prior to each pressure jump.

Using the above-mentioned approach the creep parameters (A0, Q, and n) can be obtained via only one or two (when SPS multistep pressure dilatometry is required) experiments.

3. Experimental

A commercial MoO_3 powder with a purity of 99.9% (US Research Nanomaterials, Inc., Houston, USA) was used as a raw material. The powder was wet-milled using a high energy ball milling machine (Pulverisette 6, Fritsch, Germany) run at 300 rpm for up to 30 h in air with SS304 balls (diameter: 5 mm) and jar (250 ml). The charge ratio is 12:1 for the balls and powders. Due to the small size (<500 nm) of milled MoO_3 nanopowders, the large surface tension induces the agglomeration of powders during the oven drying method. Thus, the freeze-drying method was used to prevent the agglomeration during the drying stage, and Tert-butyl alcohol (TBA) was chosen due to the high melting temperature (25 °C) and miscibility match with MoO_3 powders [20]. The milled MoO_3 powder with TBA was frozen by liquid nitrogen for 10 min and dried at −50 °C for 48 h in the freeze drier (FreeZone 1, Labconco, MO, USA). The freeze-dried MoO_3 powders were heated to 550 °C with 5 °C/min and holding for 30 min and to 850 °C with 5 °C/min and holding for 50 min or 80 min under the H_2 atmosphere, resulting in the synthesis of Mo nanopowders.

The sintering process was carried out using SPS system [21] (Dr. Sinter SPSS-515, Syntex Inc., Japan), with a tooling made from the EDM4 graphite (Poco Graphite, Inc., Texas, USA). A 0.15 mm-thick graphite paper was used to prevent adhesion between the sintered specimen and the tooling. An optical pyrometer (IR-AHS2, Chino, Japan) was used to detect the temperature (Tdie) at the 2.5 mm depth hole in the graphite die. SPS conditions for the consolidation of the H_2 reduced Mo nanopowders included the heating rate of 100 °C/min from 600 °C to the maximum temperature (950 °C and 1200 °C) with 90 MPa applied pressure and 13 min holding time. Before applying pressure and heat in SPS, the chamber was vacuumed and purged with argon gas 2 times. Then SPS experiments were conducted in argon gas. The control experiments to get the thermal expansion of the graphite die set were carried out under the same SPS conditions without Mo nanopowders.

Finding the densification mechanism requires the exact measurement of the Mo powders temperature during SPS. The temperature of the Mo nanopowders (Tsample) during SPS compaction was measured by inserting a k-type thermocouple directly into the Mo nanopowder. For the regression approach, SPS data obtained from the compaction of the Mo nanopowder at 1200 °C (Tsample = 1288 °C) were used. For the multistep pressure approach, starting with the minimum pressure, Mo nanopowders were heated up to 950 °C (Tsample = 1002 °C) with 100 °C/min. After the stabilization of the temperature during the holding stage, a few successive jumps of the pressure were applied to measure the variation of the strain rate at each pressure jump. Except for the experiments for regression analysis (section 4.2), the temperature described in this study refers to "Tdie".

X-ray diffraction (XRD) (Bruker D-8 diffractometer, MA, USA), utilizing CuKα radiation at room temperature was used to analyze the powders and compacted pellets. For the XRD, the cross-section of

the compacted pellets was grinded and polished with SiC papers and diamond paste. The densities of sintered Mo specimens were measured by the Archimedes method. The particle (or grain) size and composition were assessed by scanning electron microscopy (SEM), (FEI Quanta 450, Thermo Fisher Scientific, Waltham, USA) and Energy-dispersive X-ray spectroscopy (EDS) (Oxford Instruments, Abingdon, UK). The transverse rupture strength (TRS) of the compacted Mo pellets was measured. The experimental method to measure the TRS can be found elsewhere [22].

The plasma irradiation and reflectivity measurement conditions are explained in section 4.3 with their results.

4. Results and discussion

4.1. Fabrication of Mo nanopowders and compaction by SPS

As shown in Fig. 1(a), the as-received MoO_3 powders display a broad size distribution from 1 µm to 50 µm with plate-like particle shape. SEM images of milled MoO_3 powders in TBA are shown in Fig. 1 (b) to (d) for milling time of 3 h, 10 h and 30 h, respectively. With milling time of 30hr, an average particle size of less than 200 nm was obtained (Fig. 1(d)).
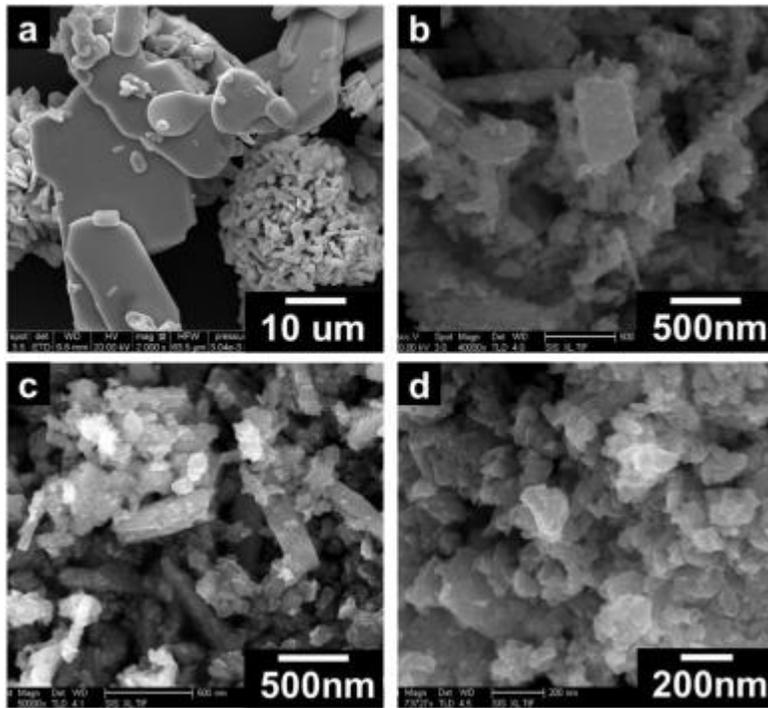

Fig. 1. SEM images of MoO_3 powders (a) without milling and with milling for (b) 3 h, (c) 10 h and (d) 30 h.

The intensity drop and the peak broadening from XRD of the MoO_3 powders [23] can indicate the decrease of the crystalline size with increasing milling time (Fig. 2(a)). The bottom graph of Fig. 2(b) shows the XRD pattern of the H2 reduced Mo powders. Using the H2 reduction method, the MoO_3 powders were successfully transformed to Mo (ICSD collection code # 76147) [24]. The XRD analysis of the Mo pellet compacted by SPS at 950 °C with 13 min holding time, 90 MPa and Ar atmosphere shows

the oxide peak (MoO2 with ICSD collection code # 01-078-1073) indicated by the green arrow in Fig. 2(b). EDS analysis with 5 points average showed that 5.16 at% oxygen was observed near the edge of Mo pellet. Otherwise, no oxygen was detected at the center of the SPSed Mo pellet. However, since the detection of oxygen is not accurate by EDS, it's possible that the center of Mo pellet has also oxygen concentration which is lower than the detection limit of EDS. Therefore, we concluded that there is more oxidation at the edge compared to the center. Before applying pressure and heat in SPS, the chamber was vacuumed and purged with argon 2 times. This step may help to remove the oxygen inside of the Mo powders. After applying pressure, some oxygen from the argon gas may start to react from the edge of the Mo pellet. SPS of Mo nanopowders in H2 atmosphere can render more homogenous Mo pellets.

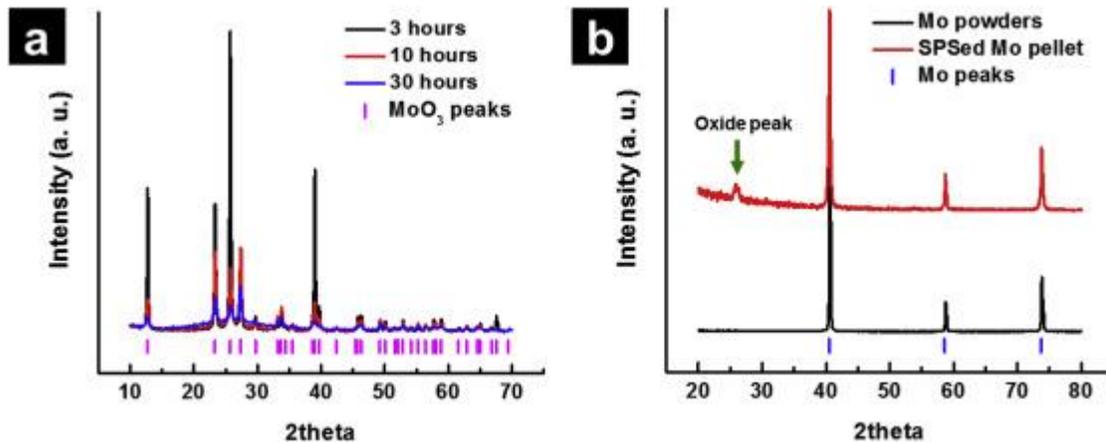Fig. 2. (a) XRD of MoO3 powders with different milling time (3 h, 10 h and 30 h). (b) H2 reduced Mo powders (bottom) and SPSed Mo pellet (top). The MoO3 and Mo reference peaks are shown at the bottom of XRD graphs. The green arrow indicates the MoO2 phase. (For interpretation of the references to colour in this figure legend, the reader is referred to the Web version of this article.)

The H2 reduced Mo powders have an average grain size of 100 nm as shown in Fig. 3(a) and (b). During the H2 reduction, Mo particles are connected by necks which are increased with the holding time at 850 °C. The morphology of Mo powders reduced at 850 °C for 80 min (Fig. 3(b)) represents a more interconnected structure compared to that of the powders H2 reduced at the same temperature for 50 min (Fig. 3(a)). The large interconnected area in the Mo powders affects the sintering kinetics of Mo compaction by enhancing the diffusion of atoms during SPS.
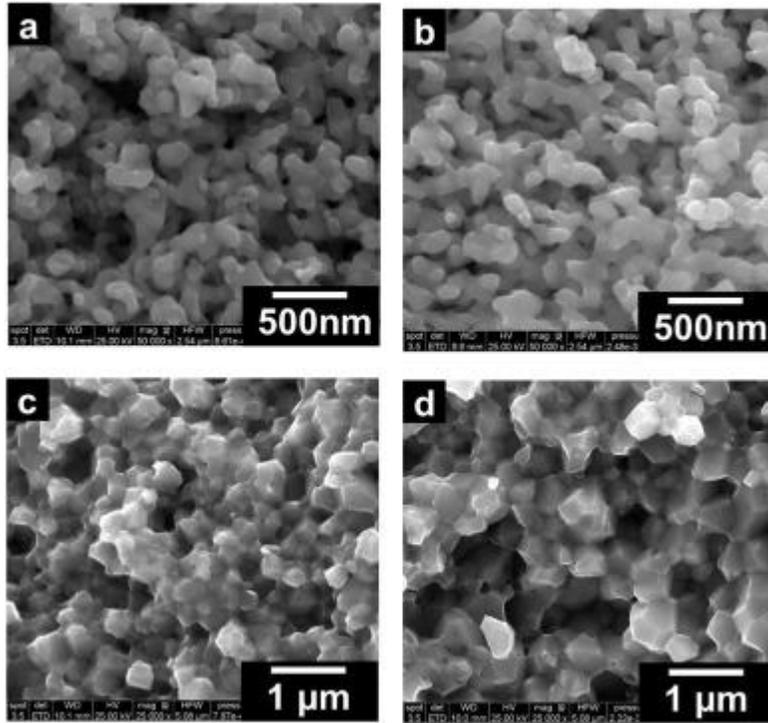
Fig. 3. SEM images of Mo powders reduced at 850 °C for (a) 50 min and (b) 80 min. SEM images of (c) Mo pellet using powder (a), and (d) Mo pellet using powder (b) compacted at 950 °C, 90 MPa, 100 °C/min and 13 min of holding time by SPS.

The H2-reduced Mo powders were consolidated with the heating condition of 950 °C, 90 MPa, 100 °C/min and 13 min of holding time using SPS. The average grain size and relative density of Mo pellets made from the Mo nanopowders synthesized using the H2 reduction time of 80 min are about 700 nm (Fig. 3(d)) and 93.89%, respectively, which are slightly higher values than 400 nm (Fig. 3(c)) and 92.58% of the Mo pellet obtained from the Mo nanopowders synthesized using the H2 reduction time of 50 min. TRS values of the Mo pellets made from the Mo nanopowders synthesized using the H2 reduction times of 50 min and 80 min are 486.27 MPa and 472.16 MPa, respectively. Higher TRS is expected for the smaller grain size Mo pellet. However, TRS is dependent on the relative density of the Mo pellet. Therefore, due to the interplay between the grain size and relative density, the Mo pellets compacted from the Mo nanopowders synthesized using the H2 reduction times of 50 min and 80 min show similar TRS values.

4.2. Densification mechanism of Mo nanopowders

The experimental SPS data (1200 °C (Tsample = 1288 °C), 90 MPa and 100 °C/min) with the ramping stage (Fig. 4(a)) was used to plot the linearization curve for various n values (1–5) shown in Fig. 4(b). The fractional relative density range from 0.41 to 0.87 is used in Fig. 4(a) to minimize the effect of the grain growth on the sintering behavior. The fitting equations for each n value are shown on the right side for each curve in Fig. 4(b). Table 1 displays the A0 and Q values for each n value for the linear regression fitting using Eq. (1) in Fig. 4(b). Fig. 4(c) shows the modeled/experimental relative density curves using

the identified sintering parameters (Table 1) and it appears that the n value is between 1 and 2. More accurate n value can be obtained by the regression of the SPS multistep pressure dilatometry data. Fig. 4(d) shows the change of the stress and height of a Mo pellet during the multistep SPS of Mo nanopowders during the isothermal holding stage of 950 °C (T sample = 1002 °C). When there is a jump of the pressure, the slope of the sample height curve is changed accordingly indicating the alteration of the strain rate for each jump. From the data in Fig. 4(d), the average n value, estimated using Eq. (2), is 1.5. Based on this n value, parameter Q value can be expected to be in the range from 150.82 kJ/mol to 192.51 kJ/mol (Table 1).
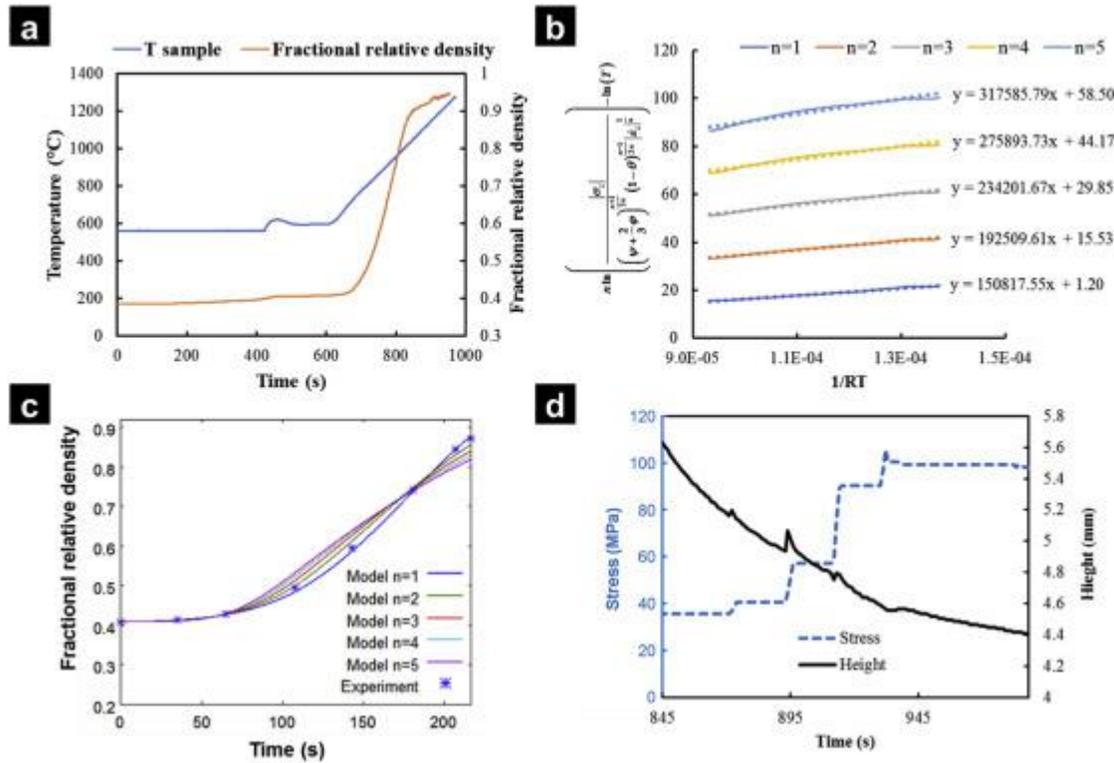

Fig. 4. The steps to find the sintering mechanism of H2 reduced Mo nanopowders compacted by SPS. (a) Experimental SPS results, (b) Linearization curves for each n values (the fitting equations are shown on the right side of each curve), (c) Modeled/experimental relative density curves using identified parameters from regression approach for each tested n values, (d) Change of applied stress and height of sample in multistep pressure method.

Table 1. Creep parameters identified from regression approach.

n	1	2	3	4	5
Q	150.82	192.51	234.20	275.89	317.59
A_0	3.007E-1	1.809E-7	1.088E-13	6.547E-20	3.939E-26

Obtained n and Q values indicate that the sintering mechanism of Mo nanopowders obtained via H2 reduction method can be Coble creep (n = 1) or grain boundary sliding (GBS) (n = 2) accommodated by diffusional flow [25] controlled by the grain boundary diffusion (Qgb = 263 kJ/mol) [26]. Due to a low

sintering temperature (0.4 Tm) imposed during SPS, the Nabarro-Herring creep (n = 1) are not possible in this case. Also, from the deformation mechanism maps by Frost and Ashby [26], we expect that the dislocation slip accommodation process for GBS (n = 2) can be suppressed since diffusional flow can be more prevalent when fine powders are sintered under low temperatures and accounting for the normalized shear strength of 0.38 used in this study. The Mo compact with average nano-size grains will have larger grain boundary area compared with that of the average micron-size grains. Therefore, the grain boundary related densification mechanism such as Coble creep or GBS is expected for the nanopowders [17]. The Q values obtained here (150.82 kJ/mol to 192.51 kJ/mol) are lower than the Qgb value (263 kJ/mol). Since the Q value is obtained from the regression fitting of the experimental porosity evolution values, it is the effective activation energy. Therefore, obtained Q value is possibly the combination of the grain boundary diffusion and the surface diffusion which is often observed for sintering of the nanopowders.

4.3. Reflectivity analysis of single crystal and nanocrystal Mo

Materials used in this experiment were SC Mo with (110) crystal orientation and NC Mo made of H2 reduced Mo powders and compacted by SPS (950 °C, 90 MPa, 100 °C/min, 13 min holding time, and Ar atmosphere). The SC and NC Mo were mechanically polished to mirror quality of approximately <0.01 μm and <0.03 μm roughness before the exposure respectively.

The SC and NC Mo disks were exposed to Ar plasma bombardment using the PISCES-A linear plasma device [27]. All samples were exposed to Ar + plasma fluxes of 3.1 × 1017/cm2s with an ion impact energy of average 85 eV. The reflectivity of the Mo samples was measured before and after exposure by high precision spectroradiometer (GS-1290-2NVIS, Gamma Scientific, USA) with the RadOMA camera and full frame lens. There is maximum 10% measurement uncertainty in the reflectivity measurement induced from the alignment angle and the surface non-uniformity of the samples.

The spectral reflectivity of the SC and NC Mo mirrors before and after exposure are displayed in Fig. 5(a). Both the SC and NC mirrors have around 70% reflectivity before plasma exposure. Under the same amount of plasma exposure, the spectral reflectivity of the SC and NC Mo mirrors was reduced approximately by 10%, but showed the comparable performance of spectral reflectivity (>∼60%). The total erosion of each sample was also measured via total mass loss analysis. Interestingly, the NC Mo mirror has 2 times higher resistance to erosion (280 nm) by plasma compared to that of the SC mirror (600 nm).
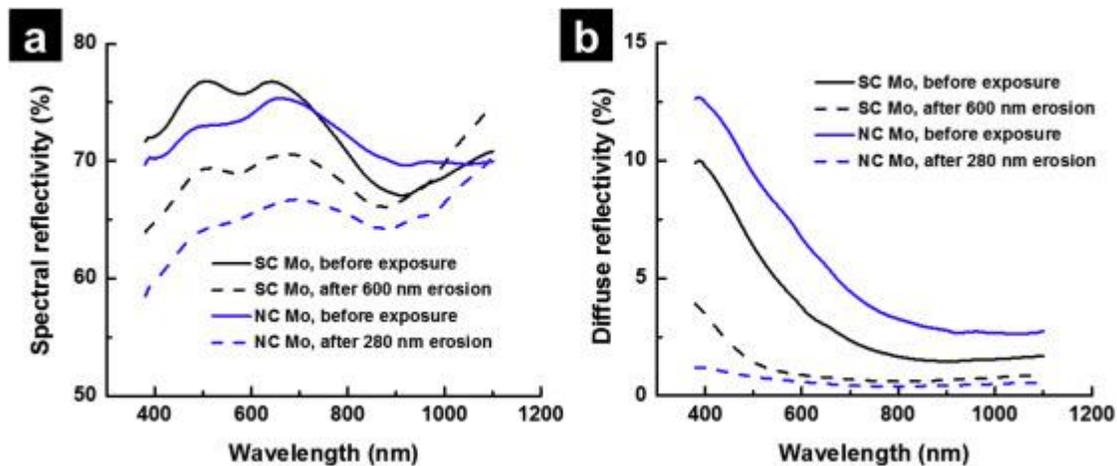
Fig. 5. (a) Spectral reflectivity of single crystal (SC) and nanocrystal (NC) Mo before and after plasma exposure (45° illuminations and 45° collection), (b) Diffuse reflectivity of SC and NC Mo and (45° illuminations and 35° collection).

The diffuse reflectivity of the NC Mo mirror used in this study is lower than that of the SC Mo mirror under the same plasma conditions. As shown in Fig. 5(b), the NC Mo mirror has a low average diffuse reflectivity of less than 1% after exposure. The high diffuse reflectivity of the SC mirror in the range of <600 nm can be related to the eroded pattern observed after exposure (right image of Fig. 6(a)). However, the surface relief formation, which is known as the main reason for the high diffuse reflectivity of polycrystalline metal mirror [8], was also observed for the SPSed Mo mirror after exposure in this study (right image of Fig. 6(b)). Therefore, the eroded pattern in SC Mo mirror affects more negatively the diffuse reflectivity compared to the surface relief pattern in NC Mo mirror in this study.
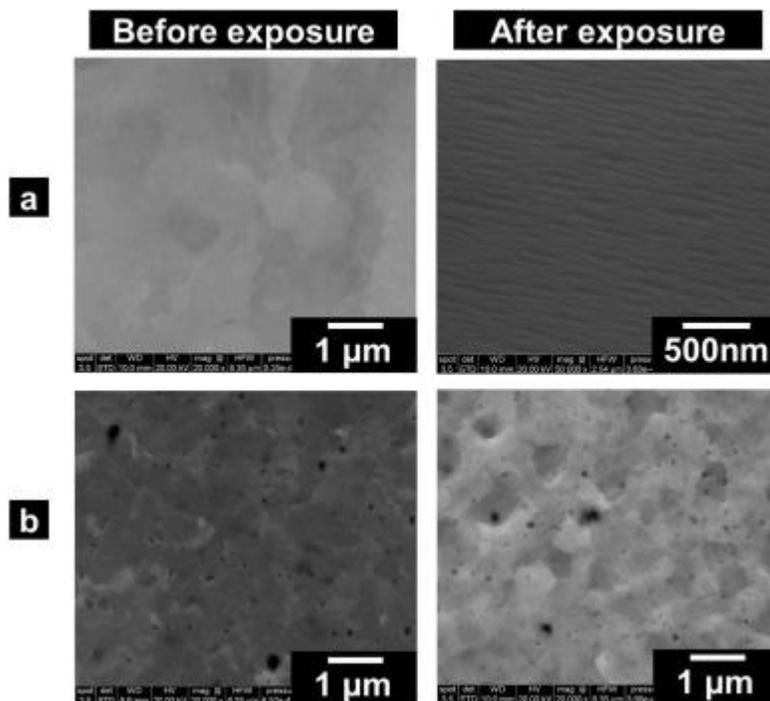
Fig. 6. SEM images of (a) single crystal (SC) and (b) nanocrystal (NC) Mo before (left) and after (right) plasma exposure.

Although maximum 10% of measurement error makes the reflectivity results ambiguous, NC Mo mirror clearly has higher erosion resistance compared to SC Mo mirror, which was not observed for the NC mirror (100 nm grain size) made by magnetron sputtering [3].

In summary, the consolidation behavior of the Mo nanopowders obtained from milled MoO_3 powders by H_2 reduction was analyzed by the regression of the experimental data on regular SPS and on the SPS multistep pressure dilatometry. Obtained creep parameter values n and Q are 1.5 and 151 kJ/mol to 193 kJ/mol, respectively, indicating Coble creep or GBS accommodated by diffusional flow controlled by grain boundary diffusion as the densification mechanism of the Mo nanopowders used in this study. The NC Mo disk shows the promise in approaching the reflectivity of the SC Mo in the as-polished condition. Initial optical test results are not conclusive due to the measurement error of the reflectivity. However, NC Mo showed good resistance to erosion compared to that of the SC Mo. The sintering of Mo alloy with the grain growth inhibitors like ZrC to achieve smaller average grain size, and more accurate optical measurements should be a focus of future studies.

5. Conclusions

For the first time, the densification mechanism of Mo nanopowders compacted by SPS was analyzed. A NC Mo metal mirror with submicron grain size fabricated by SPS was tested using a spectroradiometer after plasma exposure. The densification mechanism of the Mo nanopowders during SPS is Coble creep or the grain boundary sliding, which is expected for the fine metal nanopowders. The spectral reflectivity of the NC Mo mirror after exposure is comparable with that of the SC mirror. In particular, the NC Mo mirror shows higher erosion resistance compared with the SC Mo in this study. By further optimizing the H_2 reduction and SPS process or utilizing Mo powders alloying with the grain growth inhibitor, bulk scale NC Mo mirrors can be possibly fabricated by SPS, which should provide clear benefits in terms of cost, size and life expectancy of metal mirrors.

Acknowledgments

Data availability

The raw/processed data required to reproduce these findings cannot be shared at this time as the data also forms part of an ongoing study.

REF

[1] B. Eren, L. Marot, M. Langer, R. Steiner, M. Wisse, D. Mathys, E. Meyer, The

effect of low temperature deuterium plasma on molybdenum reflectivity,

Nucl. Fusion 51 (10) (2011) 103025.

[2] J.N. Brooks, J.P. Allain, Particle deposition and optical response of ITER

motional Stark effect diagnostic first mirrors, Nucl. Fusion 48 (4) (2008),

045003.

[3] B. Eren, L. Marot, A. Litnovsky, M. Matveeva, R. Steiner, V. Emberger, M. Wisse,

D. Mathys, G. Covarel, E. Meyer, Reflective metallic coatings for first mirrors on

ITER, Fusion Eng. Des. 86 (9) (2011) 2593e2596.

[4] M. Wisse, B. Eren, L. Marot, R. Steiner, E. Meyer, Spectroscopic reflectometry of

mirror surfaces during plasma exposure, Rev. Sci. Instrum. 83 (1) (2012),

013509.

[5] M.S. Park, T.S. Jo, S.H. Kim, D.-G. Kim, Y.D. Kim, Two-step Sintering of Molybdenum Nanopowder,
Advances in Sintering Science and Technology, John

Wiley & Sons, Inc., 2010, pp. 415e420.

[6] T. Sugie, S. Kasai, M. Taniguchi, M. Nagatsu, T. Nishitani, Irradiation test of Moand W-mirrors for ITER
by low energy deuterium ions, J. Nucl. Mater.

329e333 (2004) 1481e1485.

[7] A. Litnovsky, G. De Temmerman, K. Vukolov, P. Wienhold, V. Philipps,

O. Schmitz, U. Samm, G. Sergienko, P. Oelhafen, M. Büttner, I. Orlovskiy,

A. Yastrebkov, U. Breuer, A. Scholl, Investigations of single crystal and polycrystalline metal mirrors
under erosion conditions in TEXTOR, Fusion Eng.

Des. 82 (2) (2007) 123e132.

[8] V.S. Voitsenya, M. Balden, A.F. Bardamid, V.N. Bondarenko, J.W. Davis,

V.G. Konovalov, I.V. Ryzhkov, O.O. Skoryk, S.I. Solodovchenko, Z. Zhang-jian,

Development of surface relief on polycrystalline metals due to sputtering,

Nucl. Instrum. Methods Phys. Res., Sect. B 302 (2013) 32e39.

[9] Z. Zhou, Y. Ma, J. Du, J. Linke, Fabrication and characterization of ultra-fine

grained tungsten by resistance sintering under ultra-high pressure, Mater.

Sci. Eng. 505 (1e2) (2009) 131e135.

[10] A.P. Ilyin, O.B. Nazarenko, G.V. Shuvalov, I.V. Klekovkin, D.V. Tikhonov,

L.O. Tolbanova, Production and characterization of molybdenum nanopowders obtained by electrical explosion of wires, Optoelectron. Adv. Mater.

Rapid Commun. 4 (6) (2010) 834e837.

[11] G.-S. Kim, Y.J. Lee, D.-G. Kim, Y.D. Kim, Consolidation behavior of Mo powder

fabricated from milled Mo oxide by hydrogen-reduction, J. Alloy. Comp. 454

(1e2) (2008) 327e330.

[12] G.-S. Kim, H.G. Kim, D.-G. Kim, S.-T. Oh, M.-J. Suk, Y.D. Kim, Densification

behavior of Mo nanopowders prepared by mechanochemical processing,

J. Alloy. Comp. 469 (1e2) (2009) 401e405.

[13] C. Maniere, L. Durand, G. Chevallier, C. Estourn es, A spark plasma sintering

densification modeling approach: from polymer, metals to ceramics, J. Mater.

Sci. 53 (10) (2018) 7869e7876.

[14] C. Maniere, L. Durand, A. Weibel, C. Estourn es, Spark-plasma-sintering and

finite element method: from the identification of the sintering parameters of a

submicronic a-alumina powder to the development of complex shapes, Acta

Mater. 102 (2016) 169e175.

[15] E.A. Olevsky, Theory of sintering: from discrete to continuum, Mater. Sci. Eng.

R 23 (2) (1998) 41e100.

[16] W. Li, E.A. Olevsky, J. McKittrick, A.L. Maximenko, R.M. German, Densification

mechanisms of spark plasma sintering: multi-step pressure dilatometry,

J. Mater. Sci. 47 (20) (2012) 7036e7046.

[17] T.G. Nieh, J. Wadsworth, O.D. Sherby, Superplasticity in Metals and Ceramics, Cambridge University Press, Cambridge, 1997.

[18] W.R. Cannon, T.G. Langdon, Creep of ceramics, J. Mater. Sci. 18 (1) (1983) 1e50.

[19] G. Lee, J. McKittrick, E. Ivanov, E.A. Olevsky, Densification mechanism and mechanical properties of tungsten powder consolidated by spark plasma sintering, Int. J. Refract. Metals Hard Mater. 61 (2016) 22e29.

[20] N. Ni, M. Tesconi, S.E. Tabibi, S. Gupta, S.H. Yalkowsky, Use of pure t-butanol as a solvent for freeze-drying: a case study, Int. J. Pharm. 226 (1e2) (2001) 39e46.

[21] E.A. Olevsky, D.V. Dudina, Field-assisted Sintering: Science and Applications, Springer International Publishing, 2018.

[22] E. Khaleghi, Y.-S. Lin, M.A. Meyers, E.A. Olevsky, Spark plasma sintering of tantalum carbide, Scripta Mater. 63 (6) (2010) 577e580.

[23] H.E. Swanson, R.K. Fuyat, Natl. Bur. Stand. Circular 539 (3) (1954) 30.

[24] H.E. Swanson, E. Tatge, Standard X-Ray Diffraction Powder Patterns. Vol. I, Data for 54 Inorganic Substances, National Bureau of Standards, Washington, D.C., 1953.

[25] M.F. Ashby, R.A. Verrall, Diffusion-accommodated flow and superplasticity, Acta Metall. 21 (2) (1973) 149e163.

[26] H.J. Frost, M.F. Ashby, Deformation-mechanism Maps, the Plasticity and Creep of Metals and Ceramics, Pergamon Press, Oxford, 1982.

[27] D.M. Goebel, G. Campbell, R.W. Conn, Plasma surface interaction experimental facility (PISCES) for materials and edge physics studies, J. Nucl. Mater. 121 (1984) 277e282.